tvst

Article

Nanoscale Characteristics of Ocular Lipid Thin Films Using Kelvin Probe Force Microscopy

Elizabeth Drolle[1], William Ngo[1], Zoya Leonenko[2,3], Lakshman Subbaraman[1,*], and Lyndon Jones[1–3]

[1] Centre for Ocular Research & Education (CORE), School of Optometry & Vision Science, University of Waterloo, Waterloo, Ontario, Canada
[2] Department of Physics and Astronomy, University of Waterloo, Waterloo, Ontario, Canada
[3] Department of Biology, University of Waterloo, Waterloo, Ontario, Canada

Correspondence: Elizabeth Drolle, Centre for Ocular Research & Education (CORE), School of Optometry & Vision Science, University of Waterloo, 200 University Ave W, Waterloo, ON, N2L 3G1, Canada. e-mail: edrolle@uwaterloo.ca

Received: January 9, 2020
Accepted: May 5, 2020
Published: June 29, 2020

Keywords: meibum/meibomian gland secretion; tear film; atomic force microscopy; Kelvin probe force microscopy

Citation: Drolle E, Ngo W, Leonenko Z, Subbaraman L, Jones L. Nanoscale characteristics of ocular lipid thin films using Kelvin probe force microscopy. Trans Vis Sci Tech. 2020;9(7):41, https://doi.org/10.1167/tvst.9.7.41

Purpose: To describe the use of Kelvin probe force microscopy (KPFM) to investigate the electrical surface potential of human meibum and to demonstrate successful use of this instrument on both human meibum and a meibum model system (six-lipid stock [6LS]) to elucidate nanoscale surface chemistry and self-assembly characteristics.

Materials and Methods: 6LS and meibum were analyzed in this study. Mica-supported thin films were created using the Langmuir-Blodgett trough. Topography and electrical surface potential were quantified using simultaneous atomic force microscopy/KPFM imaging.

Results: Both lipid mixtures formed thin film patches on the surface of the mica substrate, with large aggregates resting atop. The 6LS had aggregate heights ranging from 41 to 153 nm. The range in surface potential was 33.0 to 125.9 mV. The meibum thin films at P = 5 mN/m had aggregates of 170 to 459 nm in height and surface potential ranging from 15.9 to 76.1 mV, while thin films at P = 10 mN/m showed an aggregate size range of 147 to 407 nm and a surface potential range of 11.5 to 255.1 mV.

Conclusions: This study showed imaging of the differences in electrical surface potential of meibum via KPFM and showed similarities in nanoscale topography. 6LS was also successfully analyzed, showing the capabilities of this method for use in both in vitro and ex vivo ocular research.

Translational Relevance: This study describes the use of KPFM for the study of ocular surface lipids for the first time and outlines possibilities for future studies to be carried out using this concept.

Introduction

The tear film is a highly complex mixture that is composed of two primary phases—the mucin-aqueous gel phase that lies adjacent to the corneal surface and the overlying superficial lipid layer—that collectively provide the eye with a protective and functional layer to shield the cornea, as well as ensure nutritional supply.[1] The lipid layer is 15 to 160 nm thick and is composed of both hydrophobic and hydrophilic lipids.[2,3] They serve to reduce the surface tension of water, allowing the tear film to spread thinly across the ocular surface[2] and reduce the rate of tear film evaporation from the eye.[4,5] Lipids are primarily produced in the meibomian glands, which are embedded in the tarsal plate of the superior and inferior eyelids, with the orifices opening at the eyelid margins.[6–8] These secretions are referred to as meibum.

Natural meibum is a complex mixture containing hundreds of lipid species,[8] but it is commonly modeled in vitro to allow for investigation with reduced variables; one such model is a six-lipid stock (cholesterol, cholesteryl oleate, oleic acid, oleic acid methyl

ester, triolein, and phosphatidylcholine) (6LS), which is reflective of the amphiphilic and nonpolar constituents of human meibum.[9] This simplified mixture has been used to study a number of lipid-based tear film interactions, particularly contact lens deposition.[10–14]

The nanoscale characteristics and properties (e.g., topography, lipid self-assembly, and electrostatic properties) of both natural meibum and meibum models are not fully known. To study lipid membranes and lipid self-assembly, high spatial resolution is required, which cannot be achieved using conventional light microscopy.[15] Typically, atomic force microscopy (AFM) is used to address this limitation. In AFM, a sharp probe scans over the surface of a sample and measures the forces of interaction between the tip of the probe and the surface features of the sample to produce an image of surface topography at the atomic scale.[16–19] The resolution of this technique is limited only by the sharpness of the tip used; as a result, resolution can theoretically be at the atomic level.[19,20] For imaging biological samples, intermittent contact mode is most commonly used. In this mode, the cantilever is oscillated at or near its resonance frequency and comes into intermittent contact with the surface of the sample during scanning. In contrast, sample destruction can occur in contact mode as the tip drags across the surface of the sample.[19,21,22] Using the principles of the AFM setup, different methods of scanning probe microscopy can be employed to study different physical features.[20] One such extension is the Kelvin probe force microscope (KPFM), which uses an electrically conductive AFM probe with a voltage applied to it that allows for the measurement of the contact potential difference between the tip and the surface of the sample (atop a conductive substrate) to generate a high-resolution image or map of the electrical surface potential of a sample while in noncontact mode.[23–26] This allows for the imaging of electrical surface potential distribution of biomolecules that can arise from charged molecules, the presence of polar molecules in the film, or even dipole moments.[26–28] The instrument also allows for simultaneous topography (via AFM) and electrical surface potential (via KPFM) imaging so that their relationship can be studied.[23] This method has proven valuable for studying thin films, such as lipid monolayers, lung surfactants, heterogeneity of complex mixtures, and protein and peptide interactions.[29–34]

The aim of this study is twofold. The first is to describe in detail the use of AFM and KPFM for nanoscale characterization of meibum. The second is to provide examples of the use of AFM and KPFM to successfully infer information on both natural human meibum and the simplified 6LS model to study their self-assembly and surface chemistry characteristics. To our knowledge, this is the first time that meibum has been analyzed using KPFM to show differences in electrical surface potential, which may be an important determinant in understanding the interactions of lipids with different biomolecules, as well as artificial substrates, including contact lenses.

Methods

This study was conducted in adherence to the tenets of the Declaration of Helsinki, and ethics clearance was obtained from a University of Waterloo ethics committee prior to conducting research activities (ORE #31243). Informed consent was obtained from all participants prior to enrollment in the study.

Six-Lipid Stock

The six-lipid stock described is a simplified model system for human meibum.[9] It was created by combining a mixture of triolein, cholesterol, oleic acid, oleic acid methyl ester, cholesteryl oleate, and phosphatidylcholine, with a molar ratio of nonpolar to polar lipids of 994:6 (all from Sigma Aldrich, St. Louis, MO). The mixture was made in a 1:1 hexane-ether mixture; prior to experimental analysis, the mixture was dried down and resuspended in high-performance liquid chromatography (HPLC)–grade chloroform and stored at –20°C. The 6LS mixture was prepared in concentrations as outlined in Table 1.

Participants

Meibum was collected from six healthy participants without dry eye symptoms. A presterilized titanium Mastrota paddle (OCuSOFT Mastrota Meibomian Paddle, 754-5-29; Mastrota, Rosenberg, TX) was placed nasally behind the inferior lid to retract the lower lid away from the eye while the patient looked upward.[35] Pressure was applied to the eyelid against the face of the paddle using a gloved finger, expressing the meibum from within the meibomian glands and out of the meibomian orifices at the eyelid margin. The expressed meibum was collected using a small, degreased metal ocular spud (Ellis Eye Spud, part no. K2-4100; Katena, Parsippany, NJ) by gently sweeping it over the eyelid margin. Meibum expression and collection was conducted in five locations along the lower eye lid margin for each eye, and the meibum

Table 1. Molecular and Experimental Details of the Six-Lipid Stock Used for This Study, Based on That Described by Lorentz et al.[9]

Parameters	Triolein	Cholesterol	Oleic Acid	Oleic Acid Methyl Ester	Cholesteryl Oleate	Phosphatidylcholine
Polarity	Nonpolar	Nonpolar	Nonpolar	Nonpolar	Nonpolar	Polar/amphiphilic
Solution concentration (mg/mL $CHCl_3$)	0.213	0.024	0.024	0.16	0.32	0.00667

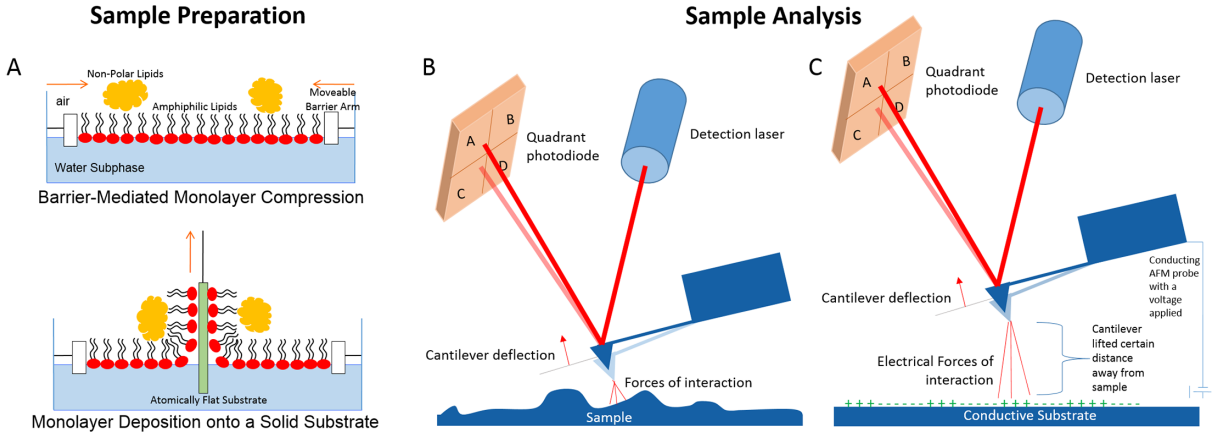

Figure 1. Illustrated depiction of sample preparation and analysis. Samples were prepared using the Langmuir-Blodgett trough (A) prior to analysis using AFM (B) and KPFM (C). AFM uses a physical probe to scan across the surface of a sample, giving topographical imaging with nanoscale resolution. KPFM is based on an AFM setup and uses a conducting AFM probe with a voltage applied to it, allowing for the mapping of local electrical surface potential in air. B and C altered from Drolle et al.[40] This figure is intended as a simplified guide and is not meant as an exact representation of the complex lipid makeup, structures, or organizations.

collected was pooled and immediately deposited in HPLC-grade chloroform and stored at –20°C prior to film preparation and analysis.

Sample Preparation on Langmuir-Blodgett Trough

Thin films of each mixture were deposited on mica substrates (Ashville-Schoonmaker Mica Co., Newport News, VA) using the Langmuir-Blodgett (LB) microtrough (KSV NIMA; Biolin Scientific, Stockholm, Sweden). Prior to sample preparation, the LB trough was thoroughly cleaned using HPLC-grade chloroform. For the trough subphase, nanopure water was used, generated using a Milli-Q Gradient A10 water system (MilliporeSigma, Burlington, MA), with a resistivity value ≥18.2 MΩ. After cleaning with chloroform, the trough was filled with nanopure water, all of which was immediately removed to remove residual impurities. The trough was then refilled with nanopure water and the pressure zeroed, and rapid isotherm analyses were performed to test for the presence of contamination and impurities. If there was a change in surface pressure greater than 0.0 ± 0.2 mN/m, the surface of the subphase was removed and the pressure sensor was rezeroed. Sample preparation with the trough was carried out within a vibration-dampened isolation chamber.

The LB trough was used for the creation of thin film samples of 6LS and meibum, facilitated with the use of chloroform. Chloroform is an organic solvent that allows samples to self-assemble once the chloroform is evaporated. This can be seen in Figure 1A, which illustrates the amphiphilic molecules arranging themselves at the air-water interface, with the polar head groups interacting with the water and the nonpolar tail groups positioned away from the water and toward the air. Nonpolar lipids then can interact with the nonpolar tails of these amphiphilic molecules to shield themselves from the water. The moveable barrier arms can be used to hold a specified pressure for the deposition of the lipid monolayers that form at the air-water interface of the trough. They will adjust accordingly to hold that pressure constant as

the dipping mechanism is operating to pass a solid substrate through the monolayer in order to collect a thin film sample.

Fresh mica was cleaved using adhesive tape. The intrinsic layered structure of mica allows it to yield an atomically flat plane as a substrate for deposition. This allows for detection of nanoscale thickness variation from samples unachievable in other substrates (e.g., glass). The mica was then attached to the dipping arm, placed into the dipping well of the trough, and submerged in the subphase. After the substrate was in place, the barrier arms were closed slightly (~15%) and the sample mixture (meibum or 6LS) was deposited in drop form gently onto the surface of the subphase. After the sample was deposited, the barrier arms were then fully opened to give additional space for the lipid molecules to self-assemble and equilibrate for 10 minutes to allow for complete evaporation of the organic solvent.

After the equilibration period, a pressure control was carried out at a pressure of 5 to 10 mN/m at a speed of 20 cm^2/min. Once the barrier arms reached the desired pressure hold, the dipping arm was moved up slowly (as seen in Fig. 1A) at a speed of 2 mm/min, with the barrier arms compressing as necessary to maintain a constant pressure to deposit a monolayer from the air-water interface of the trough onto the mica. This is the ideal method for using mica as a substrate as it is hydrophilic in nature, such that when it is raised through the monolayer, the lipid head groups interact with the surface and the tail groups point outward into the air.

In terms of deposition speed, the minimum or maximum speed should be avoided as to not push the instrument to either of its limits, where functionality may not be optimal. After deposition was complete, samples were removed from the dipping arm of the trough and stored in a desiccator for a minimum of 24 hours to ensure proper dehydration. Prior to further analysis, samples were then affixed to a metallic substrate to allow for the conductivity necessary for KPFM imaging.

Atomic Force Microscopy and Kelvin Probe Force Microscopy

Samples were imaged using intermittent contact mode AFM and noncontact mode KPFM to visualize the topography and observe the differences in surface potential. Imaging was conducted using a SmartSPM 1000 (AIST-NT, Horiba Instruments, Inc., Kyoto, Japan) scanning probe microscope in air at room temperature (20°–25°C) and normal humidity (10%-50%), using a gold-coated cantilever (HQ:NSC14-Cr-Au; μMasch USA, NanoAndMore USA Corp., Watsonville, CA) with a resonance frequency of 160 kHz and a spring constant of 5.0 N/m. The analysis started with a topography scan to optimize instrument setup and to ensure the sample was appropriately prepared for imaging. Once the sample had been established, AFM and KPFM were carried out simultaneously in a two-pass technique (forward scan = AFM at the surface using intermittent contact mode; reverse scan = KPFM in noncontact mode at a lift distance of 10.0 nm). Set point and gains were initially automatically selected for each sample and then adjusted as necessary to improve imaging quality. The scan rate was set to 0.5 to 1.0 Hz, with an image resolution of 400 × 400 pixels to 800 × 800 pixels. For each sample analyzed, images were captured at three different and independent locations with multiple different image sizes for each area to examine and ensure consistency of results across the sample. For each scan, multiple image types were gathered, including two heights, magnitude, phase (AFM), and contact potential difference. This methodology is outlined in Figure 1B (AFM) and Figure 1C (KPFM).

The specifications for the cantilever, as outlined by μMasch USA (NanoAndMore USA Corp., Watsonville, CA) are shown in Table 2.

Cantilever Selection

Cantilever selection is vital in AFM/KPFM analysis. There are numerous factors to consider, including the sharpness of the tip, the resonance frequency, and the force constant. The sharpness of the tip will indicate what can be visualized, as the limit of resolution for scanning probe microscopy methods is dictated by the sharpness of the tip. Samples smaller than the size of the tip will not be resolved, so sharp tips are ideal.[36] However, cantilevers with a coating, such as those required for KPFM to allow for electrical conductivity, cause the resulting tip radius to be larger, which is an important factor to consider when selecting a cantilever. For this work, the cantilever used had a typical radius of 8 nm when uncoated (meaning that features as small as 8 nm theoretically can be resolved); however, with the gold coating for KPFM imaging, the radius of the tip can only be confidently reported to be smaller than 35 nm.

Cantilevers must be short and thin to ensure a good signal from the laser and that low force is applied to the sample.[37] These factors affect the spring constant of the cantilever, which is a measurement of the materials' stiffness. Typically, for biological samples being analyzed in an intermittent or dynamic contact mode

Table 2. Cantilever Specifications for AFM/KPFM Analysis of Thin Films

Cantilever	Resonance Frequency (kHz)			Force Constant (N/m)			Length (μm)	Width (μm)	Thickness (μm)
	Minimum	Typical	Maximum	Minimum	Typical	Maximum			
HQ:NSC14-Cr-Au	110	160	220	1.8	5	13	120 to 130	22 to 28	1.6 to 2.6

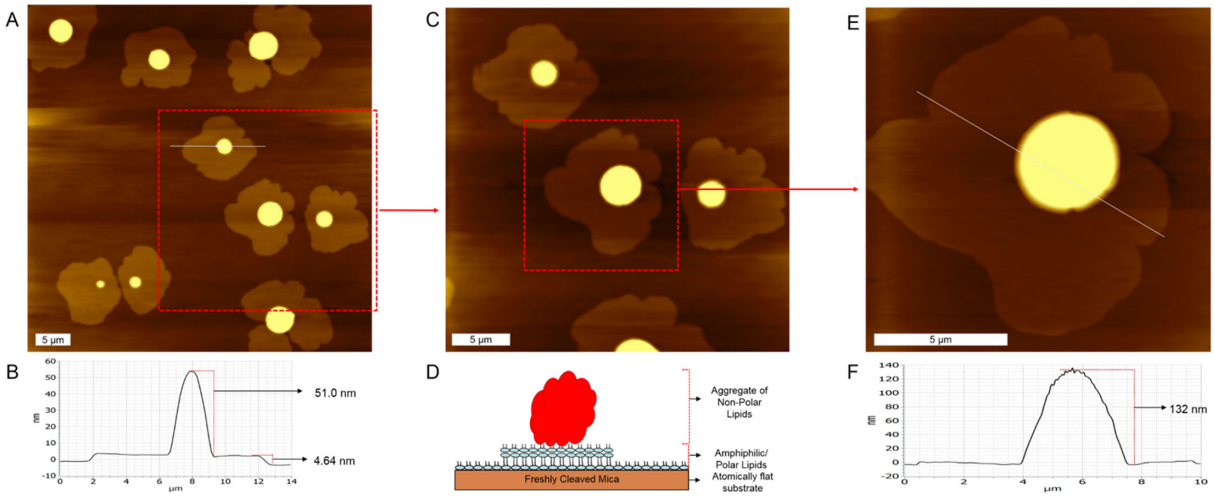

Figure 2. Representative AFM topography images of the 6LS at P = 10 mN/m, illustrating the lipid distribution in thin films deposited atop an atomically flat substrate. (A) Topography image at dimensions of 50 × 50 μm with cross section (B) marked across one surface feature. The area outlined is magnified to 30 × 30 μm (C) and further magnified to 12 × 12 μm (E). Cross sections of the highest magnification are shown in F. The most likely identity of the patches seen in the topography images is an amphiphilic lipid multilayer atop a continuous monolayer, with nonpolar lipid aggregates interacting with the nonpolar tail groups of the multilayer (D, intended as a simplified guide and is not meant as an exact representation of the complex lipid makeup, structures, or organizations).

AFM, a "soft" cantilever with a force constant of less than 5 N/m is used to avoid exerting excessive amounts of force onto the soft delicate biological sample. Intermittent contact mode preserves the integrity of the sample, as the tip taps along the surface as it scans rather than dragging across the surface in constant contact as in contact, or static, mode AFM, damaging the sample in the process. This tapping is carried out by oscillating the cantilever at or near its resonance frequency, and the higher the resonance frequency, the faster the possible scan rate. The material the cantilever is made of is also important. Although other materials can be used for the probe, typically, cantilevers are made of silicon or silicon nitride; silicon tips are stiffer and tend to be better for intermittent contact mode work; silicon nitride tips are more flexible and are commonly used in contact mode AFM and for liquid imaging.[38] For this work, the cantilevers selected were made of a silicon base, were coated in gold, and had a force constant of 5 N/m and a resonance frequency of 160 kHz.

Image Processing and Analysis

Data were processed using AIST-NT image processing software (AIST-NT Inc., Novato, CA). Topography (AFM) and contact potential difference (KPFM) images were processed using plane leveling, and lines were corrected for using fit lines, match lines, and median fit lines. Scars were removed. Quantitative measurements were obtained from raw unprocessed KPFM images. Sample size for both 6LS and meibum samples was a minimum of $n = 5$.

Data collected included topography images of the thin film samples, as well as difference in electrical surface potential maps. Quantitative information derived from the images included size of lipid patches and aggregates, heights of features, average surface roughness, and average difference in electrical surface potential.

Results

Six female participants without symptoms of dry eye were enrolled in the study, with a mean age of 39 years (median, 40 years; range, 28–59 years).

The AFM image analysis for thin films of 6LS taken at a pressure of 10 mN/m is shown in Figure 2. The samples showed irregular-shaped patches of polar lipids with large nonpolar lipid aggregates atop. Figures 2A–E illustrate three images from the

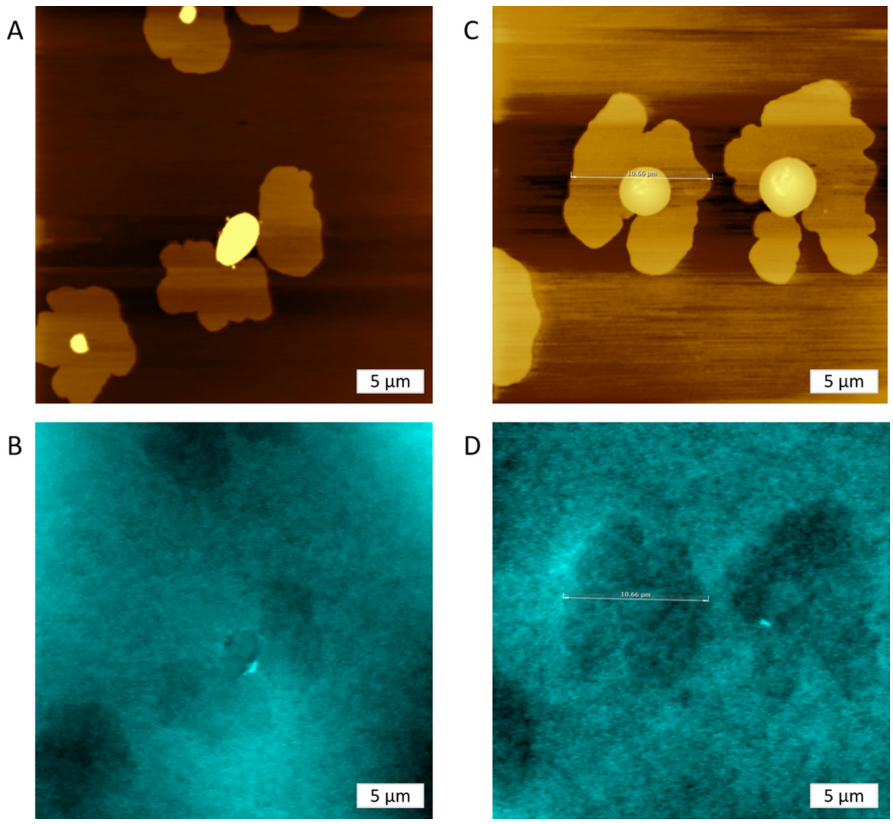

Figure 3. Simultaneous imaging of topography (*gold*) and distribution of differences in surface potential (*blue*) for 6LS thin films at P = 10 mN/m. Topographical features seen in A and C show corresponding differences in surface potential (B and D, respectively). All images taken were 30 × 30 µm.

same representative sample, with decreasing field of view (increasing magnification).

The lipid patches were between 4.0 and 5.0 nm in height (Fig. 2B). There was a large range of heights for the lipid aggregates: the aggregate in Figure 2A has a height of 51.0 nm (Fig. 2B), while the aggregate in Figure 2E has a height of 132 nm. Overall, the 6LS samples had an average surface roughness of 5.3 ± 0.3 nm and aggregates sizes ranging from 41 to 153 nm in height.

The 6LS thin film samples were simultaneously analyzed for AFM-KPFM, shown in Figure 3. Differences in electrical surface potential (KPFM) and topography (AFM) were measured simultaneously to ensure that the two images obtained correspond to the exact same location of the sample. For 6LS samples, features that are resolved in topography (Figs. 3A, 3C) have corresponding differences in surface potential (Figs. 3B and 3D, respectively). Quantitative measurements of the KPFM data showed that 6LS samples had a range of differences in electrical surface potential of 33.0 to 125.9 mV.

AFM image analysis for thin films of human meibum taken at a pressure of 5 mN/m is shown in Figure 4. The samples analyzed showed a large amount of large lipid aggregates. Figure 4 illustrates three images from the same representative sample, with decreasing image size, from 50 × 50 µm in Figure 4A to 25 × 25 µm in Figure 4B. Large aggregates (317 nm) are common, as can be visualized in Figure 4A. The cross sections of the area surrounding the large aggregates reveal areas with thickness of 4.0 to 4.5 nm (as seen in Fig. 4D, which has a thickness of 4.16 nm), indicating that lipid patches are still present with aggregates atop. These thin films showed an average surface roughness of 21.5 ± 3.1 nm and aggregate sizes ranging from 170 to 459 nm in height.

Meibum thin films taken at P = 5 mN/m were also simultaneously analyzed for AFM-KPFM, shown in Figure 5. These images also showed features in topography that correspond and align perfectly with features visible in differences in surface potential.

Quantitative measurements of the KPFM data showed that these meibum samples had a range of differences in electrical surface potential of 15.9 to 76.1 mV.

Meibum thin films were then also taken at P = 10 mN/m and analyzed for topography and difference in

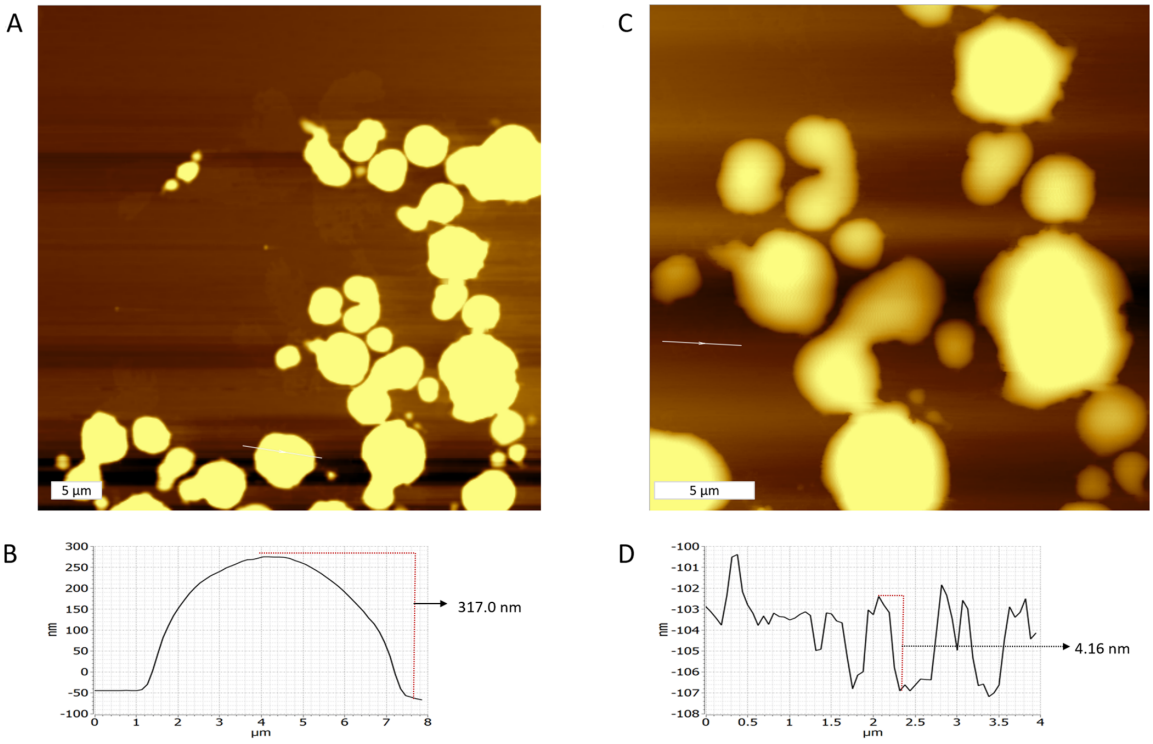

Figure 4. Representative AFM topography images of meibum at P = 5 mN/m, illustrating the lipid distribution in thin films deposited atop an atomically flat substrate. (A) Topography image at dimensions of 50 × 50 µm with cross section (B) marked across one aggregate on the surface. The area outlined is magnified to 25 × 25 µm (C) with a cross section of multilayers surrounding the aggregates illustrated via the cross section in (D), which is largely hidden due to the large nature of the aggregates.

electrical surface potential. These images also show the close correspondence of features in topography with features in electrical surface potential but also reveal differences in electrical surface potential within the large lipid aggregates that are not easily visible in the topography images (e.g., details visible in Figure 6D [KPFM] that are not as apparent in Figure 6C [AFM]). Quantitative measurements taken from these images showed aggregate sizes of 147 to 403 nm in height and a range of differences in electrical surface potential of 11.5 to 255.1 mV. Topography images showed an average surface roughness of 10.8 ± 4.1 nm.

Discussion

In this study, thin films of 6LS and meibum were made and analyzed to obtain nanoscale electrical surface potential information for these two systems. The lipid self-assembly atop an air-water interface, combined with topography and differences in electrical surface potential, was successfully studied. To our knowledge, this is the first time electrical surface potential for meibum has been investigated using KPFM. This work shows the potential of nanoscale characterization techniques for the investigation of meibum and could potentially pave the way for studies to examine meibum from individuals with ocular surface disease (e.g., meibomian gland dysfunction).

The physical features observed in the representative topography images of 6LS—lipid patches with larger lipid aggregates atop with size ranges (Fig. 2)—illustrate the necessity for a nanoscale imaging technique. These features cannot be resolved using conventional light microscopy.[28] The thickness of the lipid patches is equivalent to the approximate height of a lipid bilayer (Fig. 2D), suggesting the presence of lipid multilayers of the amphiphilic phospholipids. This would set up an environment for large aggregates of nonpolar lipids to interact together and then interact with the nonpolar tails of the phospholipids.

Meibum samples were analyzed from two difference pressures, 5 mN/m and 10 mN/m. Higher pressures may be used for deposition with the trough; however, preliminary studies (data not shown) showed that meibum has high compressibility, likely due to the large concentration of nonpolar lipids, so lower pressures were more appropriate for deposition. This agrees with results from Butovich et al.,[39] who looked at

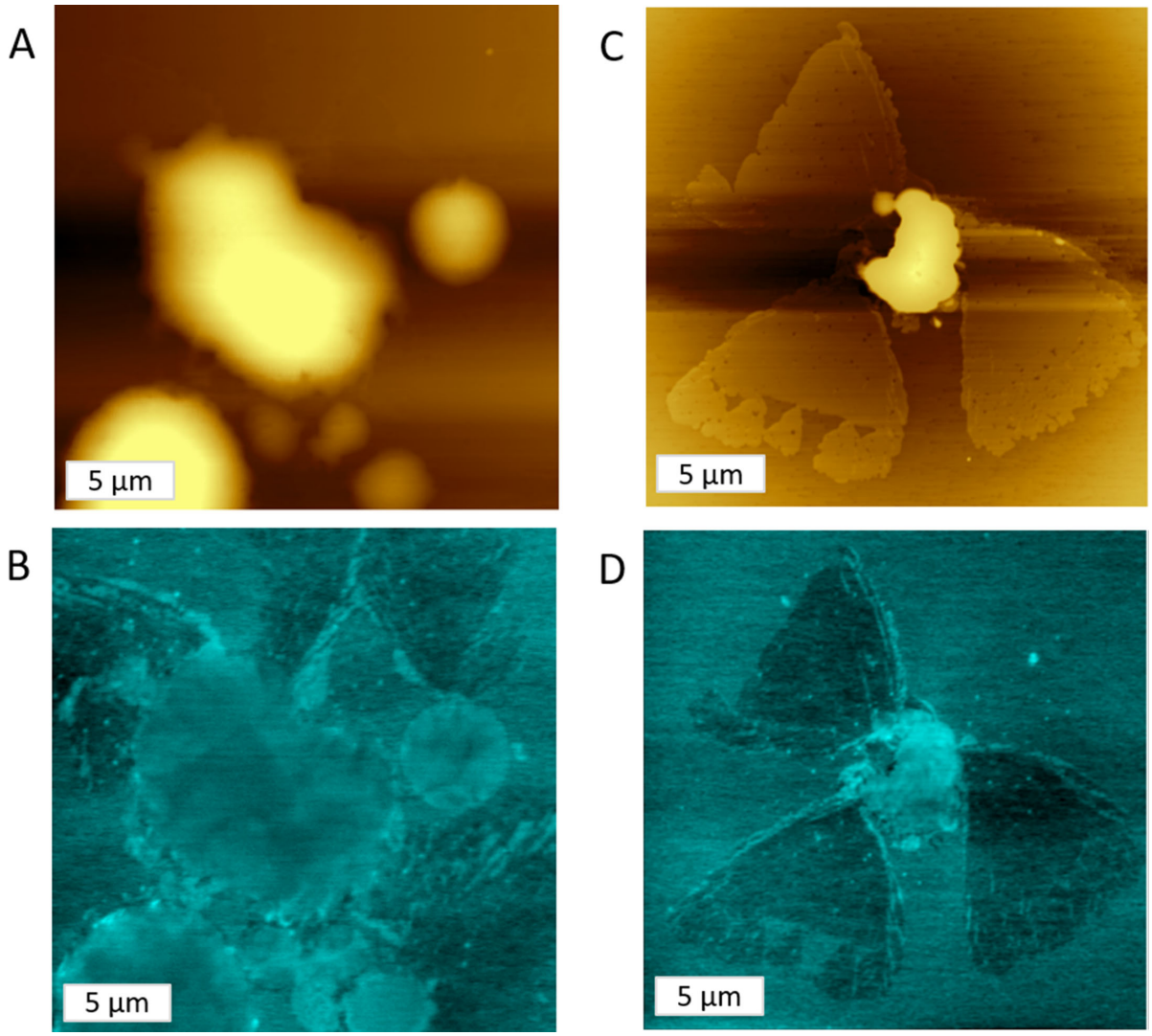

Figure 5. Simultaneous imaging of topography (*gold*) and distribution of differences in surface potential (*blue*) for meibum thin films at P = 5 mN/m. Topographical features seen in A and C show corresponding differences in surface potential (B and D, respectively). All images taken were 30 × 30 µm.

different meibum loads and the pressures they were able to reach through isotherm analysis. They observed that even with the highest meibum loads (i.e., the largest amount of meibum), pressures did not exceed 25 mN/m, while the lowest meibum loads were only able to reach pressures of approximately 7 mN/m.[39] As a result, two deposition pressures were chosen (5 mN/m and 10 mN/m) because some individuals may not express sufficient meibum to be able to compress the sample to a pressure of 10 mN/m and complete a deposition at this pressure. These results show that this type of sample preparation and analysis can still yield valuable information at lower surface pressures, like 5 mN/m, if necessary to accommodate for intersubject variability in meibum quantity. Measuring samples at lower deposition pressures results in a larger area available to the components of the mixture. This creates aggregates that are smaller in size, which decreases shielding of data and provides indirect information on nonsurface characteristics of the meibum.

The meibum samples show large nonpolar lipid aggregates, which may be attributed to the high complexity of human meibum, which can contain hundreds of individual lipid species.[8] It was relatively more difficult to observe polar lipid patches in human meibum, which were readily visible in the 6LS thin films; however, they can be faintly observed (Fig. 4A) through KPFM imaging (Fig. 5B), showing that the aggregates are atop irregular patches of multilayer lipids, similar to that of 6LS samples. This highlights the value of simultaneous KPFM/AFM imaging, where topographical information that could

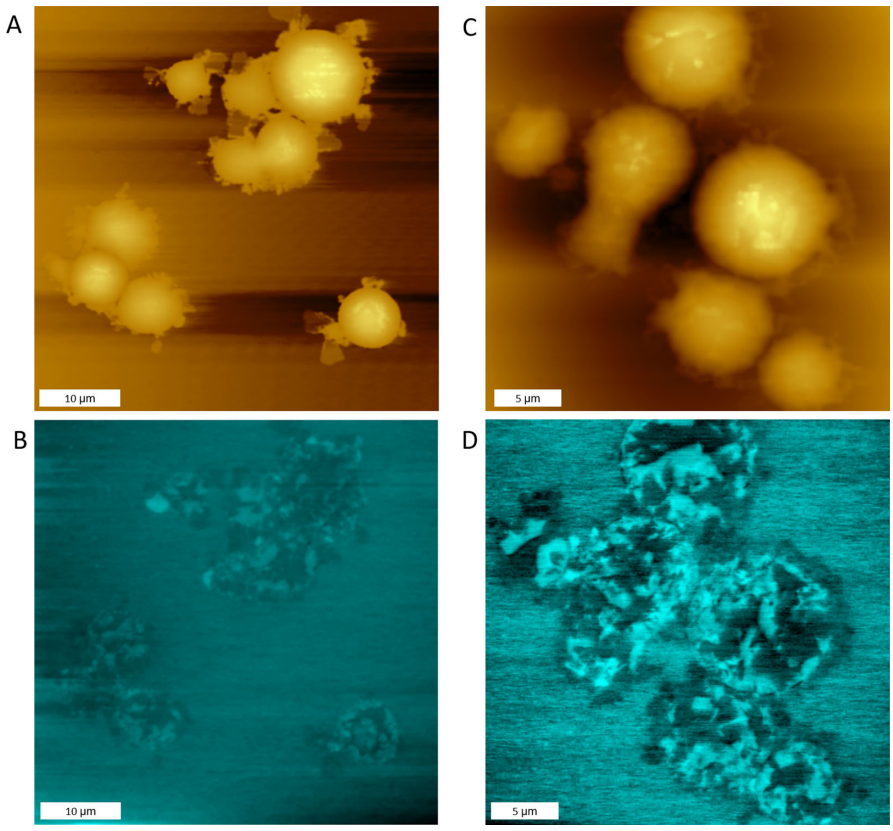

Figure 6. Simultaneous imaging of topography (*gold*) and distribution of differences in surface potential (*blue*) for meibum thin films at P = 10 mN/m. Topographical features seen in A and C show corresponding differences in surface potential (B and D, respectively).

not be resolved with AFM (i.e., limitations with color scaling) is resolved with KPFM (which is independent of topography). A possible explanation for why lipid patches were more difficult to observe in the larger-scale images (e.g., Fig. 4A, 50 × 50 µm) may be due to color assignment; brighter colors indicate higher features than darker colors. When a sample has very large surface features, the color scaling adjusts for this and essentially "hides" the smaller features from view.

The potential exhibited by lipid films from meibum or 6LS is a function of the strength of the molecular dipoles within the lipid film in a direction perpendicular to the interface, as well as the dielectric constant and packing density or area of each molecule.[32] For example, the phospholipids have contributions from various regions (i.e., head group, aliphatic tail). As such, each molecule has its own electrical surface potential distribution that can combine with others to give an electrical surface potential map. In meibum thin films (Fig. 6), KPFM imaging was able to differentiate these different groupings of molecules exhibiting their own electrical surface potential distribution within the large nonpolar lipid aggregates, providing features that were not readily apparent in the topographical imaging. This further illustrates the high image resolving capabilities of KPFM as an analytical technique for nanoscale analysis of ocular surface samples.

The differences in electrical surface potential for the meibum samples showed a smaller spread than may be expected. This could be possibly attributed to the increased complexity of the meibum system, as well as the larger number of large nonpolar aggregates present in the meibum sample. There is a lower signal for these large aggregates because they are not arranged in a lipid monolayer or multilayer. As the clusters aggregate upon themselves to shield the nonpolar lipids from the polar environment, the dipole moments are randomly distributed and may even cancel each other out, resulting in a lower signal.

Overall, the two important outcomes of this study were to describe how ocular samples could be analyzed using the KPFM and to provide experimental information for an in vitro meibum model and ex vivo human meibum. This study demonstrates the proof of principle of this technique and suggests some value for its use in vision science research, but this study was not without limitations. For example, the experiment was not conducted under physiologic temperature due

to practical limitations of the LB trough system. It may be possible the lipid patch and aggregates appear differently under such conditions, and as such, future directions for this research would include conducting the imaging under physiologic conditions (i.e., at ocular surface temperatures or in liquid). It would also be valuable to examine other in vitro models for human meibum that begin to more closely address the complexity of meibum. Next steps also include use of this technique to identify and quantify the differences between normal and "unhealthy" individuals (e.g., subjects with meibomian gland dysfunction). At the moment, this technique would be limited as a practical diagnostic tool due to various limitations, including sample preparation and analysis time. Rather, it would be an ideal technique to ascertain the surface chemistry differences between samples that can then be used to further this field of study.

This study opens the door for multiple avenues of studying meibum samples, particularly in terms of now being able to successfully investigate the differences in electrical surface potential and electrostatics. The importance of looking at the electrostatics of lipid systems lies in extrapolating from a monolayer system to look at how differences in potential on the membrane surface may affect different cellular and protein interactions.

Acknowledgments

Disclosure: **E. Drolle**, None; **W. Ngo**, None; **Z. Leonenko**, None; **L. Subbaraman**, None; **L. Jones**, Alcon (C), CooperVision (C), J&J Vision (C), Novartis (C), Ophtecs (C); **Centre for Ocular Research & Education (CORE)**, Alcon (F), Allergan (F), CooperVision (F), GL Chemtec (F), iMed Pharma (F), J&J Vision (F), Lubris (F), Menicon (F), Nature's Way (F), Novartis (F), Ote (F), PS Therapy (F), Safilens (F), Santen (F), Shire (F), SightGlass (F), Visioneering (F)

* LS is currently an employee of Alcon; was based at CORE at the time of the study.

References

1. Willcox MDP, Argueso P, Georgiev GA, et al. TFOS DEWS II tear film report. *Ocul Surf*. 2017;15:366–403.
2. Cwiklik L. Tear film lipid layer: a molecular level view. *Biochim Biophys Acta*. 2016;1858:2421–2430.
3. King-Smith PE, Hinel EA, Nichols JJ. Application of a novel interferometric method to investigate the relation between lipid layer thickness and tear film thinning. *Invest Ophthalmol Vis Sci*. 2010;51:2418–2423.
4. McCulley JP, Shine W. A compositional based model for the tear film lipid layer. *Trans Am Ophthalmol Soc*. 1997;95:79–88, discussion 88–93.
5. Bron AJ, Tiffany JM, Gouveia SM, Yokoi N, Voon LW. Functional aspects of the tear film lipid layer. *Exp Eye Res*. 2004;78:347–360.
6. Bron AJ, Tiffany JM. The meibomian glands and tear film lipids: structure, function, and control. *Adv Exp Med Biol*. 1998;438:281–295.
7. Brown SI, Dervichian DG. The oils of the meibomian glands: physical and surface characteristics. *Arch Ophthalmol*. 1969;82:537–540.
8. Butovich IA. The Meibomian puzzle: combining pieces together. *Prog Retin Eye Res*. 2009;28:483–498.
9. Lorentz H, Heynen M, Kay LM, et al. Contact lens physical properties and lipid deposition in a novel characterized artificial tear solution. *Mol Vis*. 2011;17:3392–3405.
10. Ng A, Heynen M, Luensmann D, Jones L. Impact of tear film components on lysozyme deposition to contact lenses. *Optom Vis Sci*. 2012;89:392–400.
11. Lorentz H, Heynen M, Khan W, Trieu D, Jones L. The impact of intermittent air exposure on lipid deposition. *Optom Vis Sci*. 2012;89:1574–1581.
12. Ng A, Heynen M, Luensmann D, Subbaraman LN, Jones L. Impact of tear film components on the conformational state of lysozyme deposited on contact lenses. *J Biomed Mater Res B Appl Biomater*. 2013;101:1172–1181.
13. Walther H, Lorentz H, Heynen M, Kay L, Jones LW. Factors that influence in vitro cholesterol deposition on contact lenses. *Optom Vis Sci*. 2013;90:1057–1065.
14. Walther H, Subbaraman L, Jones LW. In vitro cholesterol deposition on daily disposable contact lens materials. *Optom Vis Sci*. 2016;93:36–41.
15. Sezgin E. Super-resolution optical microscopy for studying membrane structure and dynamics. *J Phys Condens Matter*. 2017;29:273001.
16. Santos NC, Castanho MA. An overview of the biophysical applications of atomic force microscopy. *Biophys Chem*. 2004;107:133–149.
17. Engel A, Lyubchenko Y, Muller D. Atomic force microscopy: a powerful tool to observe biomolecules at work. *Trends Cell Biol*. 1999;9:77–80.

18. Frederix PL, Bosshart PD, Engel A. Atomic force microscopy of biological membranes. *Biophys J*. 2009;96:329–338.
19. Binnig G, Quate CF, Gerber C. Atomic force microscope. *Phys Rev Lett*. 1986;56:930–933.
20. Meyer E. Atomic force microscopy. *Prog Surface Sci*. 1992;41:3–49.
21. Zhang Y, Murphy KD. Multi-modal analysis on the intermittent contact dynamics of atomic force microscope. *J Sound Vibration*. 2011;330:5569–5582.
22. Water Wvd, Molenaar J. Dynamics of vibrating atomic force microscopy. *Nanotechnology*. 2000;11:192–199.
23. Nonnenmacher M, Oboyle MP, Wickramasinghe HK. Kelvin probe force microscopy. *Appl Phys Lett*. 1991;58:2921–2923.
24. Melitz W, Shen J, Kummel AC, Lee S. Kelvin probe force microscopy and its application. *Surface Sci Rep*. 2011;66:1–27.
25. Zerweck U, Loppacher C, Otto T, Grafstrom S, Eng LM. Accuracy and resolution limits of Kelvin probe force microscopy. *Phys Rev B*. 2005;71:125424.
26. Moores B, Hane F, Eng L, Leonenko Z. Kelvin probe force microscopy in application to biomolecular films: frequency modulation, amplitude modulation, and lift mode. *Ultramicroscopy*. 2010;110:708–711.
27. Rodriguez BJ, Kalinin SV. KPFM and PFM of biological systems. In: Sadewasser S, Glatzel T, eds. *Kelvin Probe Force Microscopy: Measuring and Compensating Electrostatic Forces*. Berlin, Germany: Springer Berlin Heidelberg; 2012:243–287.
28. Allison DP, Mortensen NP, Sullivan CJ, Doktycz MJ. Atomic force microscopy of biological samples. *Wiley Interdiscip Rev Nanomed Nanobiotechnol*. 2010;2:618–634.
29. Drolle E, Gaikwad RM, Leonenko Z. Nanoscale electrostatic domains in cholesterol-laden lipid membranes create a target for amyloid binding. *Biophys J*. 2012;103:L27–L29.
30. Finot E, Leonenko Y, Moores B, Eng L, Amrein M, Leonenko Z. Effect of cholesterol on electrostatics in lipid-protein films of a pulmonary surfactant. *Langmuir*. 2010;26:1929–1935.
31. Hane F, Drolle E, Leonenko Z. Effect of cholesterol and amyloid-beta peptide on structure and function of mixed-lipid films and pulmonary surfactant BLES: an atomic force microscopy study. *Nanomedicine*. 2010;6:808–814.
32. Leonenko Z, Rodenstein M, Dohner J, Eng LM, Amrein M. Electrical surface potential of pulmonary surfactant. *Langmuir*. 2006;22:10135–10139.
33. Drolle E, Negoda A, Hammond K, Pavlov E, Leonenko Z. Changes in lipid membranes may trigger amyloid toxicity in Alzheimer's disease. *PLoS One*. 2017;12:e0182194.
34. Hane F, Moores B, Amrein M, Leonenko Z. Effect of SP-C on surface potential distribution in pulmonary surfactant: atomic force microscopy and Kelvin probe force microscopy study. *Ultramicroscopy*. 2009;109:968–973.
35. Hagedorn S, Drolle E, Lorentz H, Srinivasan S, Leonenko Z, Jones L. Atomic force microscopy and Langmuir-Blodgett monolayer technique to assess contact lens deposits and human meibum extracts. *J Optom*. 2015;8:187–199.
36. Kasas S, Thomson NH, Smith BL, Hansma PK, Miklossy J, Hansma HG. Biological applications of the AFM: from single molecules to organs. *Int J Imaging Systems Technol*. 1997;8:151–161.
37. Colton RJ, Baselt DR, Dufrene YF, Green JB, Lee GU. Scanning probe microscopy. *Curr Opin Chem Biol*. 1997;1:370–377.
38. Gadegaard N. Atomic force microscopy in biology: technology and techniques. *Biotech Histochem*. 2006;81:87–97.
39. Butovich IA, Arciniega JC, Wojtowicz JC. Meibomian lipid films and the impact of temperature. *Invest Ophthalmol Vis Sci*. 2010;51:5508–5518.
40. Drolle E, Hane F, Lee B, Leonenko Z. Atomic force microscopy to study molecular mechanisms of amyloid fibril formation and toxicity in Alzheimer's disease. *Drug Metab Rev*. 2014;46:207–223.